

## Critical Role of Inelastic Interactions in Quantitative Electron Microscopy

K. A. Mkhoyan,\* S. E. Maccagnano-Zacher, M. G. Thomas, and J. Silcox

*School of Applied and Engineering Physics, Cornell University, Ithaca, New York 14853, USA*

(Received 9 June 2007; published 17 January 2008)

A semiquantitative correlation between experimental observations and theoretical prediction in electron microscopy is achieved. Experiments conducted on amorphous silicon in the convergent beam electron diffraction mode provide measurements of the reduction of the central-disk intensity. In addition to elastic scattering the effects of multiple inelastic scattering of the probe electrons were incorporated into the theory describing beam propagation through the specimen. With incorporation of the dominant plasmon scattering a better than 10% match of the theory with experiment is observed indicating the critical role of multiple inelastic scattering in quantitative electron diffraction and imaging.

DOI: [10.1103/PhysRevLett.100.025503](https://doi.org/10.1103/PhysRevLett.100.025503)

PACS numbers: 68.37.Lp, 61.05.jm, 61.05.cc, 61.43.Dq

Careful comparisons of experimental transmission electron microscopy images with simulated images led Hytch and Stobbs [1] to the conclusion that a problem exists “either in the modeling of the structure or in the electron scattering.” The problem manifests itself as reductions of the image contrast by factors of three to five in that paper and in succeeding work. Since the calculations are very successful in predicting image detail, this observation suggests that the coherent electron image intensity is a good deal smaller than anticipated; i.e., the balance between the coherent intensity and the incoherent background in electron scattering processes in thin films is not fully understood. Since then, other papers have explored various possibilities that could account for such a large discrepancy without much success [2]. These include the role of amorphous surface layers [3], phonon scattering [4], flexural modes particular to thin films [5], the lack of a “Stobbs factor” in electron interferograms [6], and a search for coherence among inelastically scattered electrons [7]. The origin of the Stobbs factor is an irksome issue, drawing wide attention as a question that must be addressed before electron scattering in these contexts can be considered fully understood. A useful step towards such a goal would be a demonstration of a reasonable accounting of absolute electron intensities in any scattering geometry. Such a benchmark could provide a basis for further progress with the problem.

Incoherence in electron scattering arises from a wide variety of origins and is typically diffuse in character. In imaging experiments, incoherence is expected to contribute to the background intensity and thus, if omitted in the calculation, to be responsible for the Stobbs factor. The Stobbs factor must be present not only in the images but also in diffraction patterns. Electron diffraction is often carried out using relative intensities [8] to analyze patterns rather than by absolute intensity measurements [9]. In this Letter we report a quantitative comparison of experimental convergent beam electron diffraction (CBED) patterns and associated calculations based on both elastic and inelastic

scattering of the incident beam electrons in scanning transmission electron microscope (STEM).

The experimental measurements of the CBED patterns were carried out in a VG HB-501 100 kV STEM that produces a focused electron probe of  $\sim 2.1$  Å with a 9 mrad convergent angle and a beam current of  $\sim 15$  pA. The microscope is equipped with a cold field emission gun, single-electron sensitive imaging detectors, and a parallel electron energy loss spectrometer (EELS). Amorphous silicon specimens were prepared by standard cross-sectional tripod polishing, using a commercially available Si [100] wafer with *a*-Si deposited on the surface. The CBED patterns were recorded using a single-electron-counting yttrium aluminum perovskite scintillator-photomultiplier system, and the dark counts were minimized by appropriately setting the discriminator level.

Figure 1 shows several CBED patterns recorded from *a*-Si at different thicknesses. To emphasize the differences between the patterns they are presented in log scale. The changes in the actual intensities of the patterns can be measured by taking line scans through the center of these patterns at different thicknesses as presented in Fig. 1(d). As can be observed from Fig. 1, as the specimen thickness increases, more and more electrons of the incident probe (central disk) scatter outside the disk thereby reducing the number of the electrons in the original 9 mrad central disk.

For quantitative analysis, the integrated intensities in the original 9 mrad disks were calculated from experimentally measured CBED patterns of the *a*-Si specimen at various thicknesses. The results were normalized to the incident electron probe, i.e., to the CBED pattern measured with no specimen [see Fig. 1(a)]. This determines the relative reductions of the original intensity. The thicknesses of the sample areas under study were estimated from recorded electron energy loss spectra using the ratios of the intensities of the single plasmon loss to the zero loss:  $t = \lambda_{pl}[I_{pl}/I_0]$ , where  $\lambda_{pl}$  is the mean-free path of plasmon generation [10]. The mean-free path of the plasmon generation in *a*-Si was measured separately using crystalline

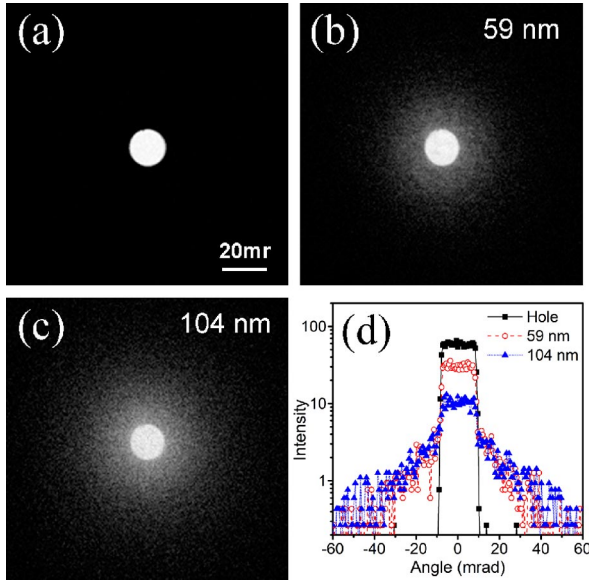


FIG. 1 (color online). CBED patterns measured from *a*-Si specimen using a 2.1 Å STEM probe with a 9 mrad convergent angle: (a) without a specimen, (b) after passing through 59 nm *a*-Si, and (c) after 104 nm (all in log scale). The images are in 0 (min)—255 (max) gray scale. (d) The actual intensities shown by line scans taken across the center of the CBED patterns.

Si as a reference [11], resulting in  $\lambda_{\text{pl}} = 1.07\lambda_{\text{pl}}^c = 128$  nm (for crystalline Si  $\lambda_{\text{pl}}^c = 120$  nm [12]).

While the formation of these CBED patterns can be described by elastic and inelastic scattering of the fast electrons of the incident beam, in crystalline specimens with periodic arrangements of the atoms and strong diffraction, tracing the history of the incident electrons becomes quite a complex problem. The set of experiments presented here provides critical simplifications of the theoretical description of the problem: the use of amorphous material allows (i) consideration of a uniform scattering potential throughout the specimen, (ii) minimal coherent elastic scattering of the electrons following inelastic collisions, and (iii) CBED patterns allow the analysis to be carried out in reciprocal space. If the thickness of a slice of the specimen,  $t = \Delta t$ , is so small that only the probability of single scattering is significant, the intensity distribution of the beam after passing through the specimen in reciprocal space can be approximated as

$$\begin{aligned} I(\vec{k}) &= I_0(\vec{k})P_{\text{el}}(t, \vec{k})P_{\text{in}}(t, \vec{k}) = I_{\text{el}}(\vec{k})P_{\text{in}}(t, \vec{k}) \\ &= I_{\text{el}}(\vec{k})[(1 - \beta) + \otimes B(\vec{k})\beta], \end{aligned} \quad (1)$$

where  $I_0(\vec{k})$  is the incident beam intensity distribution,  $P_{\text{el}}(t, \vec{k})$  and  $P_{\text{in}}(t, \vec{k})$  are the probabilities of elastic and inelastic scattering,  $I_{\text{el}}(\vec{k})$  is the intensity distribution of elastic scattered electrons,  $\otimes$  denotes convolution,  $B(\vec{k})$  [or  $B(\vec{\theta})$  using  $\lambda\vec{k} = \vec{\theta}$ ] is the angular cross section of the single inelastic scattering and can be calculated using total

cross section  $B(\vec{\theta}) = \int_0^\infty dE \frac{\partial^2 \sigma}{\partial E \partial \Omega}$ ,  $\beta$  is the probability of a single plasmon generation in the specimen with thickness  $t = \Delta t$  and can be described by Poisson statistics [10]:

$$\beta = \frac{\Delta t}{\lambda_{\text{pl}}} e^{-\Delta t / \lambda_{\text{pl}}}. \quad (2)$$

For thicker specimens with a thickness that is a multiple times  $\Delta t$ , i.e.  $t = n\Delta t$ , the expression (1) modifies into

$$\begin{aligned} I(\vec{k}) &= I_0(\vec{k})P_{\text{el}}(t, \vec{k})P_{\text{in}}(t, \vec{k})P_{\text{el}}(t, \vec{k})P_{\text{in}}(t, \vec{k}) \dots \\ &= I_0(\vec{k})[P_{\text{el}}(t, \vec{k})]^n [P_{\text{in}}(t, \vec{k})]^n \\ &= I_{\text{el}}(\vec{k})[(1 - \beta) + \otimes B(\vec{k})\beta]^n. \end{aligned} \quad (3)$$

Approximations (i) and (ii) above ensure that, once scattered inelastically, further elastic scattering will be incoherent. Thus, the effects of elastic scattering can be considered independently from the multiple inelastic scattering given by the last factor in Eq. (3).

The intensity distribution of the incident beam after passing through the specimen while scattering only elastically,  $I_{\text{el}}(\vec{k})$ , can be calculated using the multislice method. The multislice codes of Kirkland [13], which have had several successful experimental checks (see, e.g., Ref. [12]), serve as the basis for the calculations. In this computational routine, a STEM focused electron probe is first generated using optical parameters from the experimental set up: 100 kV acceleration voltage, spherical aberration coefficient of  $C_s = 1.3$  mm, objective angle of 9 mrad, and defocus of 850 Å [14]. The wave function of the STEM probe located at point  $\vec{x}_p$  is approximated as

$$\psi_p(\vec{x}, \vec{x}_p) = A_p \int_0^{k_{\text{max}}} e^{-i\chi(\vec{k}) - 2\pi i\vec{k} \cdot (\vec{x} - \vec{x}_p)} d^2\vec{k}, \quad (4)$$

where  $\lambda k_{\text{max}} = \alpha_{\text{max}}$  is the maximum angle allowed by the objective aperture,  $\chi(\vec{k})$  is the aberration function, and  $A_p$  is a normalization constant. In the multislice code the incident electron beam is then propagated through the entire thickness of the specimen by alternately passing through thin layers of the specimen and propagating between the layers. The effects of thermal vibrations of the atoms are included in the calculation by randomly displacing atoms from their sites using a Gaussian distribution with the corresponding Debye-Waller factors [12] and thus also contribute an incoherent component in the diffraction patterns. The CBED pattern is then generated by calculating the intensities of outgoing waves in reciprocal space, with an example for 109 nm *a*-Si presented in Fig. 2(a).

The amorphous layers of Si for multislice computations were constructed using a model of crystalline Si as a starting point and then displacing atoms randomly from their lattice site until the layers lose all possible periodicities, resulting in amorphous layers of Si with the same density as the crystal.

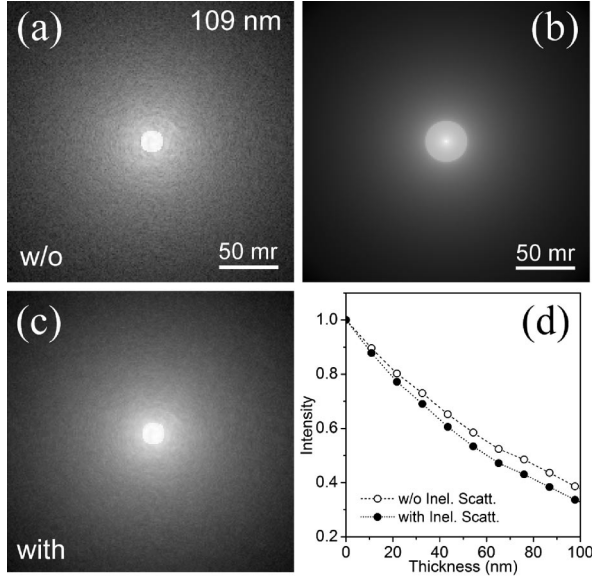


FIG. 2. CBED patterns calculated for  $a$ -Si specimen using a  $2.1 \text{ \AA}$  STEM probe with a  $9 \text{ mrad}$  convergent angle. (a) Intensity distribution of the incident beam  $I_{el}(\theta)$  after passing through  $109 \text{ nm}$  thick  $a$ -Si calculated using the multislice method where only elastic scattering of the electrons is taken into consideration (including phonons); (b) calculated cross section of the plasmon generation  $B(\theta)$  using expression (5) with  $E_{P,0} = 16.9 \text{ eV}$ ,  $\Delta E_P = 4.0 \text{ eV}$ , and  $\gamma = 3.0$ ; (c) the result in (a) after including inelastic scattering  $I(\theta)$ . The images are in log scale and in 0 (min)—255 (max) gray scale. (d) The decrease of the intensity of the beam in the original  $9 \text{ mrad}$  disk as a function of specimen thickness calculated with and without incorporation of the inelastic scattering.

To provide a first approximation to the inelastic scattering of the probe electrons, the dominant plasmon loss is considered [15]. The cross section of single bulk plasmon generation by a fast electron that loses energy  $E$  and scatters to the angle  $\theta$  can be expressed as [16,17]

$$\frac{\partial^2 \sigma}{\partial E \partial \Omega} = \frac{D}{2\pi^2 n a_0} \frac{1}{E_0} \frac{1}{\theta^2 + \theta_E^2} \times \frac{E \Delta E_P E_{P,0}^2}{[E^2 - E_{P,0}^2 - 4\gamma E_{P,0} E_0 (\theta^2 + \theta_E^2)]^2 + E^2 \Delta E_P^2}, \quad (5)$$

where  $D$  is the normalization constant,  $n$  is the atomic density of the specimen,  $a_0$  is the Bohr radius,  $E_0$  is the incident electron energy,  $\theta_E$  is the characteristic angle with relativistic correction,  $E_{P,0}$  and  $\Delta E_P$  are the plasmon energy at  $\theta = 0$  and the damping coefficient, and  $\gamma$  is dispersion coefficient. Here the plasmon dispersion relation  $E_P = E_{P,0} + 2\gamma E_0 (\theta^2 + \theta_E^2)$  was taken into consideration. Note that Eq. (5) also includes single electron valence excitations [16]. A significant drop of the cross section with increasing scattering angle is observed. It should be noted that for very thin specimens, typically  $< 10 \text{ nm}$ ,

where the bulk plasmon scattering is not the dominating mechanism, the inelastic scattering caused by surface excitations must be included.

The reduction of the intensities in the  $9 \text{ mrad}$  zero disks of the original incident beam at different thicknesses of the  $a$ -Si specimen were calculated as follows: first, the elastic scattering of the incident probe electrons for the entire thickness of the specimen was calculated using the multislice method with  $1.92 \text{ \AA}$  slices, and then inelastic scattering was added via expression (3) with the values for the probabilities of scattering calculated using expressions (5) and (2). The separation of elastic and inelastic scattering allows the use of different critical thicknesses for each type of scattering. The thickness of each slice for inelastic scattering was chosen to be  $\Delta t = \lambda_{pl}/16 = 8 \text{ nm}$  ensuring primarily single inelastic scattering in each layer [18]. This also allows a more accurate account of multiple scattering for the entire thickness of specimen. These calculations provided the rate at which the coherent incident electron waves in the probe become incoherent by *both* elastic and inelastic scattering. The only coherent intensity remaining in the problem is that which remains in the incident probe itself. The case for  $109 \text{ nm}$   $a$ -Si is presented in Figs. 2(a)–2(c). Some parameters for  $a$ -Si were taken from [19]. The reductions of the integrated intensities of the central disk calculated with and without plasmon scattering are presented in Fig. 2(d). Stronger reduction is observed when inelastic scattering is taken into account. As was expected, the effects of incorporating inelastic scattering becomes more and more substantial as the specimen thickens.

With the intensities of the central disk normalized to the intensity of the original beam, recorded by positioning the beam outside of the specimen (in vacuum), the reduction as a function of thickness independent of the incident beam current is readily seen. This method, therefore, allows direct comparison of experimentally measured values with theoretical predictions. The results of two independent experiments conducted on different  $a$ -Si specimens are presented in Fig. 3(a). The convergent angle of the incident beam in the first experiment was  $9 \text{ mrad}$  and  $8 \text{ mrad}$  in the second, while all other parameters were identical in both experiments. With the smaller convergence angle, a faster decrease of intensity with thickness should be expected, since more elastically and/or inelastically scattered probe electrons will scatter outside of the central disk. The results of the corresponding calculations carried out for both experimental conditions are presented in Fig. 3(a). The discrepancies between experimental data and numerical simulations are analyzed by calculating the divergence of the theoretical results from measured values. The discrepancies for the curves calculated with and without incorporation of inelastic scattering are presented in Fig. 3(b). Omitting inelastic scattering from the calculations results in a discrepancy between the model and experiment of about 30%. This is the Stobbs factor for

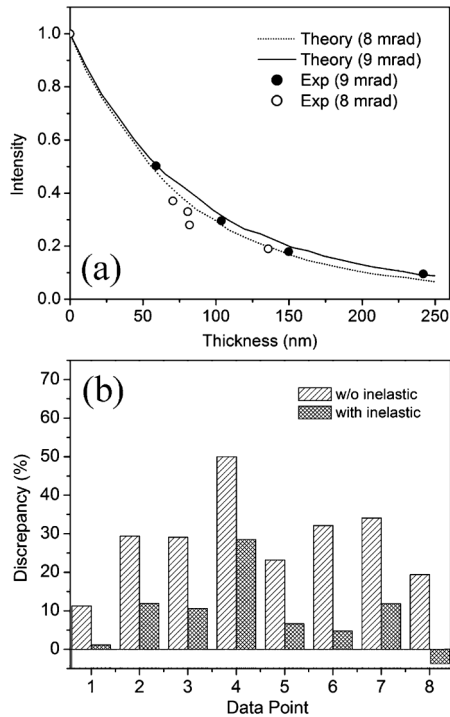


FIG. 3. (a) Reduction of the intensities in the 9 and 8 mrad central disks of the incident beam with increase of the specimen thickness and the theoretical predictions. Here both elastic and inelastic scattering of the beam electrons are included. The results of the two experiments were conducted on different *a*-Si specimens. (b) Analysis of the discrepancies between measurements and theory with and without incorporation of inelastic scattering.

the diffraction experiment and is markedly less than that reported for imaging experiments. With incorporation of the inelastic scattering, a good correlation is observed with a difference between experiment and theory of  $\leq 10\%$ . The remaining small discrepancies could be attributed to the following: not all electronic excitations are considered in the calculations, some  $\text{SiO}_x$  is expected to be present on the surfaces of the *a*-Si and limitations in the calculations due to finite pixilation of the diffraction pattern.

In conclusion, it is shown that the simplicity of the experimental arrangement of recording CBED patterns in amorphous material, combined with single-electron-detection sensitivity of the measurements carried out in STEM, provides a direct comparison of experimental data with theory. The results of the comparison identify the critical role of multiple inelastic scattering, dominated by plasmon scattering, in a quantitative description of the incident beam propagation through electron transparent specimens. Any theoretical diffraction patterns and, therefore, high-resolution images also must contain inelastic scattering for an absolute intensity comparison with experiment.

This work is supported primarily by the Nanoscale Science and Engineering Initiative of the NSF Grant No. EEC-0117770, NYSTAR Grant No. C020071, and by Cornell University. The sample preparation facilities and STEM are supported by NSF through DMR 9632275. We would also like to acknowledge Dr. E. J. Kirkland for helpful discussions.

\*Corresponding author.

kam55@cornell.edu

- [1] M. J. Hytch and W. M. Stobbs, *Ultramicroscopy* **53**, 191 (1994).
- [2] C. B. Boothroyd, *J. Microsc.* **190**, 99 (1998).
- [3] C. B. Boothroyd, R. E. Dunin-Borkowski, W. M. Stobbs, and C. J. Humphreys, *Mater. Res. Soc. Symp. Proc.* **354**, 495 (1995).
- [4] C. B. Boothroyd and M. Yeadon, *Ultramicroscopy* **96**, 361 (2003).
- [5] A. Howie, *Ultramicroscopy* **98**, 73 (2004).
- [6] H. Lichte, *Phil. Trans. R. Soc. A* **360**, 897 (2002).
- [7] R. A. Herring, *Ultramicroscopy* **106**, 960 (2006).
- [8] For example, in a recent paper [J. M. Zuo *et al.*, *Science* **300**, 1419 (2003)] the central beam of the electron beam was “obtained from the amplitude of the Fourier transform of a low resolution image.”
- [9] J. C. H. Spence and J. M. Zuo, *Electron Microdiffraction* (Plenum, New York, 1992).
- [10] R. Egerton, *Electron Energy Loss Spectroscopy in the Electron Microscope* (Plenum, New York, 1996).
- [11] A cross-sectional specimen with side-by-side crystalline and amorphous layers of Si is used. Low-loss EELS spectra were measured in both materials at the same thickness. The mean-free path of plasmon generation can be calculated as  $\lambda_{pl}^a = \lambda_{pl}^c [I_{pl}/I_0]_c [I_0/I_{pl}]_a$ . Several experiments were conducted at different thicknesses to ensure reproducibility of the results.
- [12] R. F. Loane, P. Xu, and J. Silcox, *Acta Crystallogr. Sect. A* **47**, 267 (1991).
- [13] E. J. Kirkland, *Advanced Computing in Electron Microscopy* (Plenum, New York, 1998).
- [14] The electron optical conditions of the STEM were measured on the adjacent crystalline Si sample.
- [15] P. Hirsch, A. Howie, R. Nicholson, D. W. Pashley, and M. J. Whelan, *Electron Microscopy of Thin Crystals* (Krieger, Malabar, 1977).
- [16] R. H. Ritchie and A. Howie, *Philos. Mag.* **36**, 463 (1977).
- [17] K. A. Mkhoyan, T. Babinec, S. E. Maccagnano, E. J. Kirkland, and J. Silcox, *Ultramicroscopy* **107**, 345 (2007).
- [18] In specimens with thickness  $\Delta t = \lambda_{pl}/16$  the ratio of probabilities for single to double plasmon generation, described by Poisson statistics, is  $\beta_1/\beta_2 = 2[\lambda_{pl}/\Delta t] = 32$ .
- [19] H. Raether, in *Excitation of Plasmons and Interband Transitions by Electrons*, Springer Tracts in Modern Physics Vol. 88, edited by G. Höhler (Springer-Verlag, Berlin, 1980).